Design of fractional-order controller for trajectory tracking control of a non-holonomic autonomous ground vehicle

Article (Accepted Version)

J Control Autom Electr Syst
DOI 10.1007/s40313-015-0214-2

Design of Fractional-Order Controller for Trajectory Tracking Control of a Non-holonomic Autonomous Ground Vehicle

Auday Al-Mayyahi[1] · **Weiji Wang**[1] · **Phil Birch**[1]

Received: 6 May 2015 / Revised: 5 August 2015 / Accepted: 24 September 2015

Abstract A robust control technique is proposed to address the problem of trajectory tracking of an autonomous ground vehicle (AGV). This technique utilizes a fractional-order proportional integral derivative (FOPID) controller to control a non-holonomic autonomous ground vehicle to track the behaviour of the predefined reference path. Two FOPID controllers are designed to control the AGV's inputs. These inputs represent the torques that are used in order to manipulate the implemented model of the vehicle to obtain the actual path. The implemented model of the non-holonomic autonomous ground vehicle takes into consideration both of the kinematic and dynamic models. In additional, a particle swarm optimization (PSO) algorithm is used to optimize the FOPID controllers' parameters. These optimal tuned parameters of FOPID controllers minimize the cost function used in the algorithm. The effectiveness and validation of the proposed method have been verified through different patterns of reference paths using MATLAB–Simulink software package. The stability of fractional-order system is analysed. Also, the robustness of the system is conducted by adding disturbances due to friction of wheels during the vehicle motion. The obtained results of FOPID controller show the advantage and the performance of the technique in terms of minimizing path tracking error and the complement of the path following.

✉ Auday Al-Mayyahi
Auday.almayyahi@sussex.ac.uk

Weiji Wang
W.J.Wang@sussex.ac.uk

Phil Birch
P.M.Birch@sussex.ac.uk

[1] School of Engineering and Informatics, University of Sussex, Chichester 1 Room 012, Falmer, Brighton BN1 9QJ, UK

Keywords Autonomous ground vehicle · Fractional-order PID controller · Trajectory tracking · Particle swarm optimization · Robustness · Stability

1 Introduction

The trajectory tracking problem of AGV has taken a considerable attention over the past few years. Recently, many researchers have developed various path tracking control methods considering the non-holonomic constraints of autonomous ground vehicles. In the current state of the art, many control methods and adaptive output feedback systems are emerged for solving trajectory tracking problem Huang et al. (2014). Such methods have used feedback signals to obtain a closed-loop control system based on a plant model. In Peng et al. (2014), Peng et al. derived a kinematic controller of the mobile platform to obtain a desired velocity by designing a Lyapunov function. In addition, a robust adaptive tracking controller was proposed. According to the Lyapunov stability theory, the derived robust adaptive controller guarantees global stability of the closed-loop system. In Zhang et al. (2014), Zhang et al. developed a new control approach for trajectory tracking of mobile robots. This control approach was designed based on a global finite-time control law of the angular velocity. The simulation results demonstrated a good convergence and performance to stabilize the angle error of mobile robots. In Normey-Rico et al. (2001), Juan presented a classic PID controller for path tracking problem of a mobile robot. A new PID tuning method was proposed based on basic control tools, which takes into account the robustness of the closed-loop system. In Resende et al. (2013), Resende et al. proposed a fuzzy controller for trajectory tracking with unicycle-like mobile robots. In this controller, two Takagi–Sugeno (TS) fuzzy blocks were used to generate its gains.

Published online: 06 October 2015

The stability of the developed controller was proven, using the theory of Lyapunov. In Wang et al. (2011), an adaptive trajectory tracking method based on the kinematics model was proposed to solve the non-holonomic restriction problem of trajectory tracking of the wheeled mobile robot. This method is based on the idea of the artificial field to improve the effect of the trajectory tracking. Zhao et al. (2012) produced an approach to formulate path tracking problem of an autonomous vehicle. This vehicle is a two degree of freedom. The produced approach is based on an adaptive PID controller.

Fractional-order PID (FOPID) controllers are increasingly becoming a popular technique that has gained increasing attention in recent years in industrial applications. In Aboelela et al. (2012), a FOPID controller was designed to control the trajectory of the flight path of six degree of freedom flying body. In Aldair and Wang (2010), Aldair and Wang designed an optimal FOPID controller for a full vehicle nonlinear active suspension system. In this system, the optimal values of the FOPID controller parameters for minimizing the cost function are tuned using an evolutionary algorithm. In Zamani et al. (2009), an application of FOPID controller was presented for controlling an automatic voltage regulator. This controller employed particle swarm optimization (PSO) algorithm to carry out the design procedure of FOPID.

The FOPID technique has parameter-based structure, and its performance is robust for uncertainties in robotics systems. It is apparent that FOPID controller could involve many optimization techniques for tuning and obtaining optimal parameters. In Lee and Chang (2010), Lee and Chang presented two optimization algorithms for optimizing a FOPID controller. These algorithms are an electromagnetism and evolutionary algorithm. Hence, a combination of the two algorithms was introduced to take the advantages of both algorithms and reduce the computation complexity of the electromagnetism algorithm.

In Cao et al. (2005), an intelligent optimization method is presented for designing fractional-order controllers based on genetic algorithms. The optimization design process based on genetic algorithm is analysed to obtain the proportional gain, integral gain, derivative gain, derivative order and integral order. Furthermore, the PSO has been regarded widely as a promising optimization algorithm due to its combination of simplicity (in terms of its implementation), low computational cost and good performance. Concomitantly, the optimal problems solved by genetic algorithms can obtain better solutions with PSO in comparison with conventional methods. These are precisely the main motivations that led us to apply PSO for FOPID controllers design to obtain the optimal parameters Ramezanian and Balochian (2013); Cao and Cao (2006).

Accordingly, in our earlier paper Al-Mayyahi et al. (2015), the trajectory tracking problem of autonomous ground vehicles was investigated using the proposed FOPID. The FOPID is optimized by using a particle swarm algorithm. The latter was utilized for searching the optimal values for controller's parameters. Those parameters are pivotal in designing the FOPID controller. Both of kinematic and dynamic models are used, and thus, a robust FOPID tuning is required. The tuning method is used in PSO based on the integral square of the error method (ISE) method. In this paper, the three tasks have been achieved: firstly, the analysis of actuation model and integrating it with kinematic and dynamic models. The actuation model of the AGV is an essential part in the practical performance for driving the wheels. Therefore, it is necessary to be considered into calculations and cannot be ignored. Secondly, the stability of the entire system has been inspected based on Nyquist criteria to verify the behaviour of operation region. In this paper, the system is multi-input multi-output (MIMO), and the transfer function of the system is fractional order as a result from fractional-order controller. Finally, disturbances have been applied to test the robustness of the system. The simulation results are proved that the proposed technique was successfully capable of achieving trajectory tracking. The system is globally asymptotically stable and robust to the applied external disturbances. The proposed FOPID controller has been compared with the conventional PID controller to demonstrate the advantage of using FOPID controller over the conventional method. The comparison showed that the tracking error has been minimized and improved significantly.

The rest of the paper is organized as follows: The modelling of an autonomous ground vehicle is given in Sect. 2. The explanation of the fractional-order systems is described in Sect. 3. The particle swarm optimization is demonstrated in Sect. 4. The implementation of the proposed methodology and the block diagram is depicted in Sect. 5. The stability of the fractional-order system is analysed in Sect. 6.The conducted simulation results are presented in Sect. 7 to illustrate the effectiveness of the control scheme and to validate the robustness of the fractional-order system. Finally, conclusion is drawn in Sect. 8.

2 Modelling of an Autonomous Ground Vehicle

The modelling for wheeled autonomous vehicle will be described in sections below. This modelling includes analysis for both of the kinematic and dynamic models. The kinematic model describes the motion of the vehicle without considering the forces that cause this motion. In contrast, the dynamic model takes into consideration the forces that cause the motion. The schematic diagram of the autonomous ground vehicle is depicted in Fig. 1.

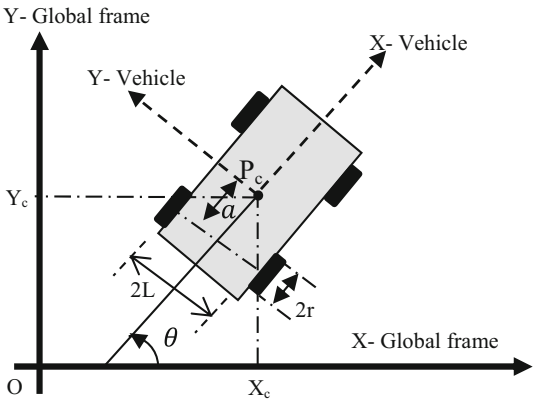

Fig. 1 The schematic diagram of the autonomous ground vehicle

2.1 Kinematic Model

The kinematic analysis of differentially wheeled autonomous vehicle in a two-dimensional plane can be conducted by using Cartesian coordinates. It is assumed that the autonomous vehicle moves without slipping on a plane, that means there is a pure rolling contact between the wheels and the ground and also there is no lateral slip between the wheel and the plane. The vehicle has four fixed standard wheels and is differentially driven by skid-steer motion. The two driving wheels are independently driven by two motors to acquire the motion and orientation. The wheels have same radius 'r'. The driving wheels are separated by distance '$2L$'. The posture of the vehicle in the two-dimensional plane at any instant is defined by the situation in Cartesian coordinates and the heading with respect to a global frame of reference. The configuration of the vehicle is represented by generalized coordinates, Pc = (X_c, Y_c, θ).

The relationships for kinematic model of the autonomous ground vehicle can be given as follows Al-Mayyahi et al. (2014):

The kinematic in the vehicle frame is given by the following equations:

$$\begin{bmatrix} \dot{x} \\ \dot{y} \\ \dot{\theta} \end{bmatrix} = \begin{bmatrix} \frac{r}{2} & \frac{r}{2} \\ 0 & 0 \\ \frac{r}{L} & -\frac{r}{L} \end{bmatrix} \begin{bmatrix} \omega_r \\ \omega_l \end{bmatrix} \tag{1}$$

$$v = r.\left[\frac{\omega_r + \omega_l}{2}\right] \tag{2}$$

$$\dot{\theta} = r.\left[\frac{\omega_r - \omega_l}{L}\right] \tag{3}$$

The kinematic in the world frame is given by the following equations:

$$\begin{bmatrix} \dot{x} \\ \dot{y} \\ \dot{\theta} \end{bmatrix} = \begin{bmatrix} \cos\theta & 0 \\ \sin\theta & 0 \\ 0 & 1 \end{bmatrix} \begin{bmatrix} v \\ \omega \end{bmatrix}$$

$$\dot{x_c} = v\cos\theta \tag{4}$$

$$\dot{y_c} = v\sin\theta \tag{5}$$

$$\dot{\theta} = \omega \tag{6}$$

$$\omega_r = \dot{\emptyset}_r \tag{7}$$

$$\omega_l = \dot{\emptyset}_l \tag{8}$$

In additional, it is assumed that the autonomous vehicle is subject to the kinematic constraints such as the contact between the wheels and the ground is pure rolling, and non-slipping Fierro and Lewis (1998).

No slip constraint

$$\dot{y_c}\cos\theta - \dot{x_c}\sin\theta = a\dot{\theta} \tag{9}$$

Pure rolling constraint

$$\dot{x_c}\cos\theta + \dot{y_c}\sin\theta + L\dot{\theta} = r\dot{\emptyset}_r \tag{10}$$

$$\dot{x_c}\cos\theta + \dot{y_c}\sin\theta - L\dot{\theta} = r\dot{\emptyset}_l \tag{11}$$

These constraints show that the driving wheels do not slip. The three non-holonomic constraints can be written in the following form:

$$A(q)\,\dot{q} = 0 \tag{12}$$

$$A(q) = \begin{bmatrix} -\sin\theta & \cos\theta & -a & 0 & 0 \\ \cos\theta & \sin\theta & L & -r & 0 \\ \cos\theta & \sin\theta & -L & 0 & -r \end{bmatrix} \tag{13}$$

$$\dot{q} = \left[\dot{x_c}\ \dot{y_c}\ \dot{\theta}\ \dot{\emptyset}_r\ \dot{\emptyset}_l\right]^T \tag{14}$$

The above system can be transformed into a more compact representation for control and simulation purposes. In this transformation, we are trying to find a way to eliminate the constraint term from the equation. The kinematic matrix is defined by the following transformation:

$$\dot{q} = \begin{bmatrix} \dot{x_c} \\ \dot{y_c} \\ \dot{\theta} \\ \dot{\emptyset}_r \\ \dot{\emptyset}_l \end{bmatrix} = \begin{bmatrix} \cos\theta & -a\sin\theta \\ \sin\theta & a\cos\theta \\ 0 & 1 \\ \frac{1}{r} & \frac{L}{r} \\ \frac{1}{r} & -\frac{L}{r} \end{bmatrix} \begin{bmatrix} v \\ \omega \end{bmatrix} \tag{15}$$

where,
v = velocity of the moving vehicle
θ = moving vehicle orientation
ω_r = angular velocity of right wheel
ω_l = angular velocity of left wheel
ω = angular velocity of vehicle.

This model is referred to a vehicle's kinematic model since it describes the velocities but not the forces or torques that have effect on the velocity. In the next section, the dynamic model will be analysed.

2.2 Dynamic Model

The dynamics model of an autonomous ground vehicle represents the study of the relationship between the various forces action on a robot mechanism and their accelerations. This is mainly used for simulation study and analysis of vehicle's design and a motion controller design for the vehicle. The description of the mechanism of the robot movement is given in terms of its component parts; bodies, joints and the parameters that characterize them. In fact, several parameters are required to define the dynamic model of a given rigid body such inertia, centre of mass and applied forces. The energy-based Lagrangian approach can be used to derive the dynamic model of the autonomous vehicle which is represented in the following general form Fierro and Lewis (1997):

$$M\left(q\right)\dot{\omega}+C\left(q,\dot{q}\right)\omega+F\left(\dot{q}\right)+G\left(q\right)=B\left(q\right)T \tag{16}$$

where $M\left(q\right)$ is the symmetric positive definite inertia matrix, $C(q,\dot{q})$ is the centripetal and Coriolis matrix, $F(\dot{q})$ is the surface friction matrix, $G(q)$ is the gravitational vector, $B(q)$ is the input transformation matrix, T is the input vector. The vehicle planar motion leads to the elimination of the gravity terms in the dynamic equation:

$$G\left(q\right)and F\left(\dot{q}\right)=0 \tag{17}$$

Therefore, Eq. (16) can be rewritten in another appropriate way as follows:

$$\overline{M}(q)\dot{\omega}+\overline{C}\left(q,\dot{q}\right)\omega=B\left(q\right)T \tag{18}$$

The above equations represent the dynamic equations of the robot considering the non-holonomic constraints, and they can be transformed into the following simplified matrix equations:

$$\begin{bmatrix} m & 0 \\ 0 & ma^2+I_c \end{bmatrix}\begin{bmatrix} \dot{w} \\ \ddot{\theta} \end{bmatrix}+\begin{bmatrix} 0 & -ma\dot{\theta} \\ ma\dot{\theta} & 0 \end{bmatrix}\begin{bmatrix} w \\ \dot{\theta} \end{bmatrix} = \frac{1}{r}\begin{bmatrix} 1 & 1 \\ L & -L \end{bmatrix}\begin{bmatrix} T_r \\ T_l \end{bmatrix} \tag{19}$$

The matrices elements are stated as follows:

$$\overline{M}\left(q\right)=\begin{bmatrix} m & 0 \\ 0 & ma^2+I_c \end{bmatrix} \tag{20}$$

$$\overline{C}\left(q,\dot{q}\right)=\begin{bmatrix} 0 & -ma\dot{\theta} \\ ma\dot{\theta} & 0 \end{bmatrix} \tag{21}$$

$$B\left(q\right)=\frac{1}{r}\begin{bmatrix} 1 & 1 \\ L & -L \end{bmatrix} \tag{22}$$

The relevant physical parameters of the autonomous vehicle are shown in Table 1:

Table 1 The parameters of autonomous ground vehicle

Parameter	Description	Value	Unit
r	Wheel radius	0.1	m
L	The distance between the drive wheel and the axis of symmetry	0.60	m
a	The distance between the centre of mass and drive wheel axis	0.25	m
m	The mass of the vehicle with driving wheels and DC motors	20	kg
I_c	The mass moment of inertia about the centre of mass	4	kgm^2

2.3 Actuation Model

An actuator is an electrical motor that drives a mechanical part of a robotic mechanism. The actuator receives a control signal directly from a control system to drive wheels into a specified motion. A DC motor is used as an actuator in this work. The model of DC motor is given in the following equations:

$$T_{\mathrm{m}}=k_{\mathrm{m}}i_{\mathrm{a}} \tag{23}$$

$$v_{\mathrm{b}}=k_{\mathrm{b}}\omega_{\mathrm{m}} \tag{24}$$

$$E_{\mathrm{a}}=R_{\mathrm{a}}i_{\mathrm{a}}+L_{\mathrm{a}}\frac{di_{\mathrm{a}}}{dt}+v_{\mathrm{b}} \tag{25}$$

$$J_{\mathrm{m}}\frac{d\omega_{\mathrm{m}}}{dt}+b_{\mathrm{m}}\omega_{\mathrm{m}}+T_{\mathrm{L}}=T_{\mathrm{m}} \tag{26}$$

where
w_{m} = The angular speed of the motor,
i_{a} = The motor current,
E_{a} = The applied voltage to the motor,
v_{b} = The back e.m.f. voltage,
J_{m} = The motor inertia,
T_{m} = The motor torque,
T_{L} = Load torque.

The physical parameters of the actuator are given in Table 2:

3 Fractional-Order Systems

In the last two decades, researchers reported that factional-order systems for modelling various materials more adequately than conventional techniques. The fractional-order systems have main effect over the controller system behaviour, for instance, to increase the speed of the response, and decrease the steady-state error and relative stability Monje et al. (2010).

Table 2 The parameters of actuator

Parameter	Description	Value	Unit
R_a	The resistance of the armature winding	8	Ω
L_a	The inductance in the motor winding	0	Henry
J_m	The motor inertia	0	kgm^2
k_m	The torque constant	0.35	N m/A
k_b	The back e.m.f. constant	0.35	V s/rad
b_m	Viscous friction	0	N m s

3.1 Fractional-Order Calculus

Fractional calculus is a mathematical topic which studies the ability of taking real number power of both the differential and integration operators. There are several definitions to describe the fractional derivative. The firmly established definitions are Grunwald–Letnikov definition and the Riemann–Liouville definition. The most frequently used definition in fractional-order calculus is the Riemann–Liouville definition, in which the fractional-order integration is defined as follows:

$$ {}_{\alpha}D_t^{-\beta} f(t) = \frac{1}{\Gamma(\beta)} \int_{\alpha}^{t} (t-\tau)^{\beta-1} f(\tau)\, d\tau \tag{27} $$

where β represents the real order of the differential and integral ($0<\beta>1$); α is the initial time instance, often assumed to be zero; and t is the parameter for which both of the differential and integral are taken. The Laplace and Fourier transforms of the fractional derivative of f (t) are given by:

$$ L\left[D_t^{\beta} f(t)\right] = S^{\beta} L[f(t)] - \sum_{k=1}^{n} S^{k} [D_t^{\beta-k-1} f(t)]_{t=0} \tag{28} $$

For convenience, the second part on the right-hand side of Eq. (28) can be ignored when the derivatives of the function f (t) are all equal to 0 at t=0. Therefore, this equation can be rewritten as follows:

$$ L\left[D_t^{\beta} f(t)\right] = S^{\beta} F(s) \tag{29} $$

where F(s) is the Laplace transformer of f(t).

3.2 Fractional-Order PID Controller

The integral–differential equation defining the control action of a fractional-order PID controller is given by

$$ u(t) = K_p e(t) + K_i D^{-\lambda} e(t) + K_d D^{\mu} e(t) \tag{30} $$

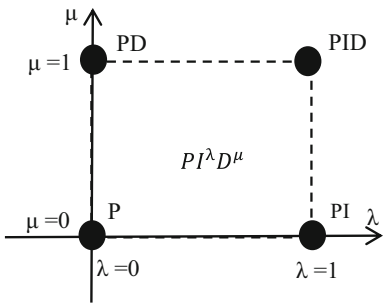

Fig. 2 Generalized FOPID controller

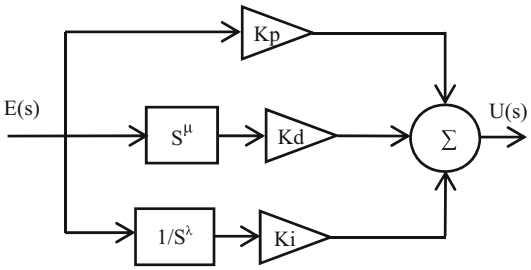

Fig. 3 The block diagram of fractional order

Applying Laplace transform to this equation with null initial conditions, the transfer function of the controller can be expressed by:

$$ C_f(s) = K_p + \frac{K_i}{S^{\lambda}} + K_d S^{\mu} \tag{31} $$

In a graphical way, the control possibilities using a fractional-order PID controller are shown in Fig. 2, extending the four control points of the classical PID to the range of control points of the quarter-plane defined by selecting the values of λ and μ.

The essential advantage of the fractional-order PID controller is the less sensitivity to changes that might happen to parameters of a controlled plant. In fact, the two extra degrees produce more adjustment for the dynamic behaviour of the fractional-order PID controller than a conventional case. The Simulink block diagram configuration of fractional-order PID controller is depicted in Fig. 3.

4 Particle Swarm Optimization

The PSO is a stochastic algorithm based on principles of natural selection and search algorithm. This algorithm is inspired by the study of birds and fish flocking. In PSO algorithm, each particle in the swarm represents a solution to the problem and it is defined with its position and velocity. In D-dimensional search space, the position of the ith particle can be represented by a D-dimensional vector, $S_i = (X_{i1}, \ldots, X_{iD})$. The velocity of the particle V_i

can be represented by another D-dimensional vector $V_i = (V_{i1}, \ldots, V_{iD})$. The best position visited by the ith particle is denoted as $\text{pbest}_i = (P_{i1}, \ldots, P_{iD})$, and gbest as the index of the particle visited the best position in the swarm; thus, gbest becomes the best solution found so far Zhang et al. (2013). The working of PSO algorithm is explained in the following procedures:

Step 1: The algorithm parameters such as a number of generations, swarm size, inertia weight minimum, maximum ($W_{\min}$, $W_{\max}$) and maximum iterations are initialized.

$$w = w_{\max} - \frac{(w_{\max} - w_{\min})}{\text{iter}_{\max}} \tag{32}$$

Step 2: The values of K_p, K_i and K_d are initialized randomly within the optimal range of values for each gain. **Step 3:** The fitness of each particle is evaluated using the integral of the square of the error (ISE). This fitness function is given as in Eq. (33).

$$\text{ISE} = \left(\int_0^\infty [e\,(t)]^2 dt \right) \tag{33}$$

Step 4: The local best position (pbest_i) and the global best position (gbest) of particles are obtained based on the fitness value calculated from procedure 3 for each particle. **Step 5:** In each iteration, the velocity and position of the particle are updated using Eqs. (34) and (35), respectively.

$$V_i^{k+1} = W V_i^k + C_1 R_1 \left(\text{pbest}_i + S_i^k \right) + C_2 R_2 \left(\text{gbest}_i + S_i^k \right) \tag{34}$$

$$S_i^{k+1} = S_i^k + V_i^{k+1} \tag{35}$$

where R_1 and R_2 are random numbers selected between 0 and 1.

Step 6: The procedures from 2 to 5 are repeated until the maximum iterations reached or the best solution is obtained.

The variables used in the PSO algorithm and their definitions are listed in Table 3.

The flow chart for particle swarm optimization is given Fig. 4:

Table 3 The definitions of the PSO variables

Variable	Definition
k	Iteration number
$\text{Iter}_{\max}$	Maximum number of iteration
D	Dimension search space
S_i^k	The current position of particle ith at iteration k
V_i^k	The current velocity of particle ith at iteration k
pbest_i	Local best position y visited by ith particle
gbest	Global best position visited by a warm
W	Inertia weight function
$W_{\max}$	Maximum value of inertia weight
$W_{\min}$	Minimum value of inertia weight
C_1	Cognitive coefficient
C_2	Social coefficient
R_1 & R_2	Random number between 0 and 1

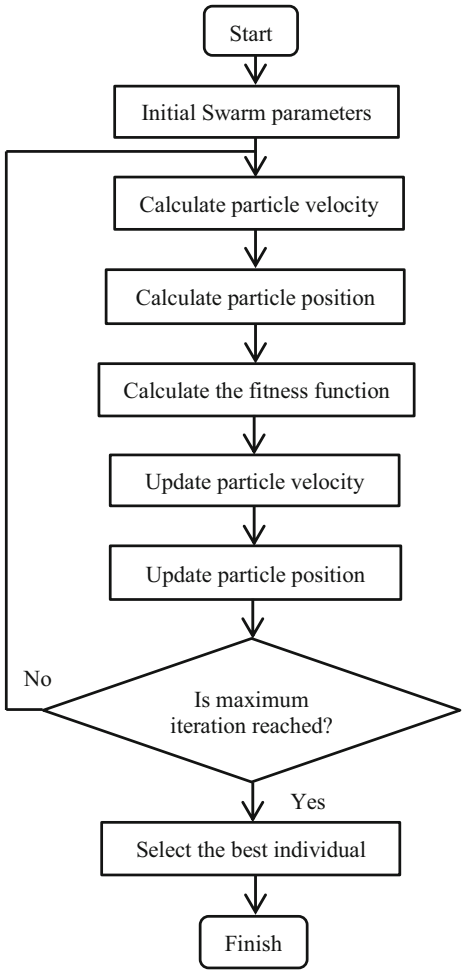

Fig. 4 The flow chart of a particle swarm optimization

5 Control System Design and Implementation

The block diagram of the AGV control system for trajectory tracking of autonomous ground vehicle is depicted in Fig. 5. Two FOPID controllers are used for driving the autonomous ground vehicle's wheels separately. The first controller receives the difference between the desired generated trajectory and actual instantaneous trajectory as an input. Therefore, the vehicle must change its orientation frequently to track the desired trajectory. The output is for controlling the right wheel. The second controller experiences the difference between the desired and actual velocity as input.

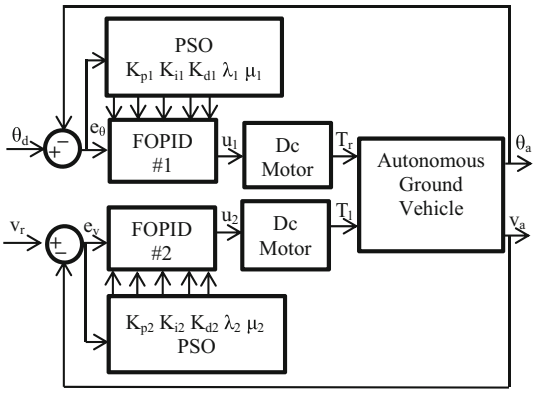

Fig. 5 The block diagram of the AGV control system

Table 4 Parameters of the FOPID controller for orientation controller

Parameters	K_{p1}	K_{i1}	K_{d1}	λ_1	μ_1
Optimal value	8.58	0.36	10.71	1.12	0.5

Table 5 Parameters of the FOPID controller for the velocity controller

Parameters	K_{p2}	K_{i2}	K_{d2}	λ_2	μ_2
Optimal value	3.35	4.33	1.23	0.89	1.10

The desired velocity was represented by a constant value. The outputs of both controllers are fed to the actuators of the autonomous ground vehicle for controlling the motion and tracking the given trajectories.

The fitness function used in PSO algorithm is simulated by using the integral square of the error method shown in Eq. (36).

$$\text{ISE} = \left(\int_0^\infty [e_\theta(t)]^2 dt\right) + \left(\int_0^\infty [e_v(t)]^2 dt\right) \tag{36}$$

The heading error signal and velocity error signal of first and second fractional-order PID are given in equations as follows, respectively:

$$e_\theta = \theta_d - \theta_a \tag{37}$$

$$e_v = v_d - v_a \tag{38}$$

where θ_d = the desired orientation, θ_a = the actual orientation, e_θ = the orientation error, v_d = the desired velocity, v_a = the actual velocity, and e_v = the velocity error.

The optimal values for the orientation and velocity controllers are given in Tables 4 and 5, respectively.

From the two tables above, the fractional-order transfer functions for the first and second FOPID controller are given as follows, respectively:

$$F_1(s) = \frac{1.23s^{1.99} + 3.35s^{0.89} + 4.33}{s^{0.89}}$$

$$F_2(s) = \frac{10.71s^{1.62} + 8.58s^{1.12} + 0.36}{s^{1.12}}$$

6 Stability Analysis

In this section, the stability analysis of the proposed system will be investigated. Different methods can be utilized to test the stability of a given system such as using Nyquist stability criterion. The latter is based on Cauchy's theorem, which is concerned with mapping contours in the complex s-plane. The Nyquist stability criterion states that the system is asymptotically stable if all its poles in are placed in the left-hand plane (LHP) and the Nyquist diagram does not enclose the point '−1'. In Vivero and Liceaga-Castro (2008), multi-input multi-output (MIMO) MATLAB toolbox was proposed for analysing the stability of multivariable systems. However, this toolbox cannot be applied for fractional-order systems. In this paper, the MIMO system is connected with two diagonal fractional-order controllers. Therefore, the total transfer function will be fractional-order transfer function. The interconnection between the MIMO loops with fractional-order controllers is shown in Fig. 6.

$F_1(s)$ and $F_2(s)$ are the two designed fractional-order PID controllers. G_{11}, G_{12}, G_{21} and G_{22} are the transfer functions of the system. These transfer functions are driven form the equations given in Sect. 2. The framework of the total closed-loop transfer functions is obtained based on individual channels design for multivariable system Ugalde-loo et al. (2005). The latter is decomposed into an equivalent set of single-input single-output (SISO) systems. Each SISO system is the open-loop channel transmittance between output $Y_i(s)$ and input $R_i(s)$ with all internal loop closed.

The multivariable system depicted above is a transfer function 'G(s)', which comprises 2x2 sub-systems, and the

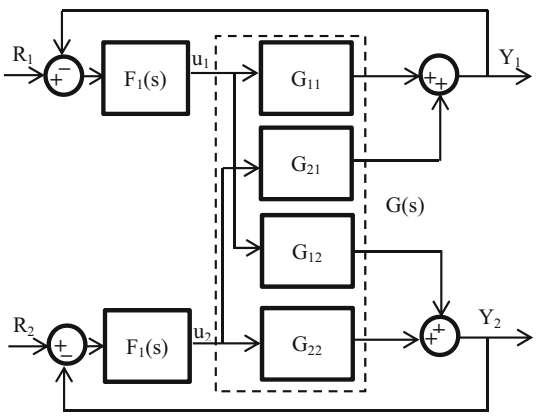

Fig. 6 Multivariable system with two controllers

controllers are $F_i(s) = \text{diag}[F_1(s), F_2(s)]$. The transfer function for each individual channel can be established as in the following relationships:

$$C_i(s) = \frac{Y_i(s)}{R_i(s)} \ (i = 1, 2) \tag{39}$$

where $C_1(s)$ *is* the first individual channel that can be defined in the following equation:

$$C_1(s) = \frac{Y_1(s)}{R_1(s)} = F_1(s)\, G_{11}(s)(1 - \gamma(s)\, H_2(s)) \tag{40}$$

Similarly for the second individual channel, $C_2(s)$ is given as follows:

$$C_2(s) = \frac{Y_2(s)}{R_2(s)} = F_2(s)\, G_{22}(s)(1 - \gamma(s)\, H_1(s)) \tag{41}$$

where $\gamma(s)$ is the multivariable structure function, and $H_i(s)$ is a unity negative feedback subsystem, which are, respectively, defined in equations as follows:

$$\gamma(s) = \frac{G_{12}(s)\, G_{21}(s)}{G_{11}(s)\, G_{22}(s)} \tag{42}$$

$$H_i(s) = \frac{F_i(s)\, G_{ii}(s)}{1 + F_i(s)\, G_{ii}(s)} \ (i = 1, 2) \tag{43}$$

The stability assessment for SISO fractional-order transfer function (FOTF) for the first individual channel '$C_1(s)$' was carried out based on MATLAB function written in reference Chen et al. (2009). In this function, a returned argument factor calls 'K' is used to determine the stability of the fractional-order system, if K is '1' the system is stable and '0' for unstable. Also, from the pole positions shown in Fig. 7, it is clearly apparent that all poles are placed with the stable region.

Figure 8 shows the Nyquist plot for first individual channel. The stability can be assessed based on Nyquist stability criterion. From the figure, it can be noticed that Nyquist diagram does not enclose the point '−1'.

The frequency-domain response can be obtained for fractional-order transfer function by replacing the variable 's' by $j\omega$. Figure 9 depicts the frequency response for the SISO fractional-order function of the first individual channel.

Similarly, the stability assessment for SISO fractional-order transfer function is performed for the second individual channel '$C_2(s)$'. Also, the returned argument factor 'K' for '$C_2(s)$' is obtained when the simulation was executing. K indicates '1' which means the system is stable. Figure 10 describes that all poles are placed in the stable region. In additional, from Fig. 11, readers can notice that Nyquist diagram does not enclose the point '−1'. Finally, the frequency-domain response is presented in Fig. 12.

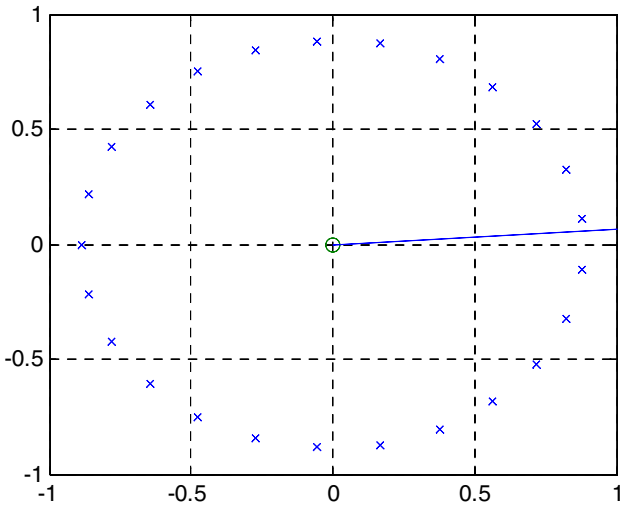

Fig. 7 Pole positions for the first individual channel

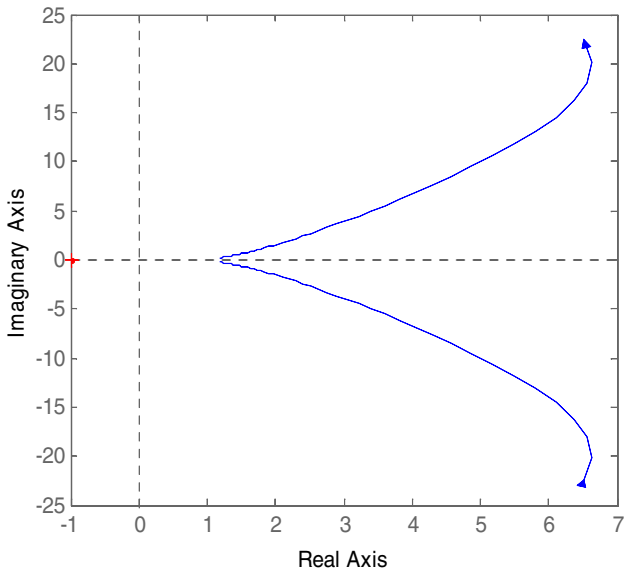

Fig. 8 Nyquist graph for first individual channel

7 Simulation Results

The simulation results are carried out to validate the proposed fractional-order PID controllers. The autonomous ground vehicle's model is governed by the kinematic and dynamic and actuating equations given in Sect. 2. The entire system has two FOPID controllers, and each controller has five parameters. These parameters are symbolized as K_{p1}, K_{i1}, K_{d1}, λ_1 and μ_1 for the first FOPID controller and as K_{p2}, K_{i2}, K_{d1}, λ_2 and μ_2. Particle swarm optimization was used in order to find the optimal values for those ten parameters. The parameters of the PSO used in the simulation are as follows: $W_{max} = 1$, $W_{min} = 0.25$, swarm size = 5, $\text{Iter}_{max} = 5$, $D = 10$, and finally both $c_1 \& c_2 = 1.4$.

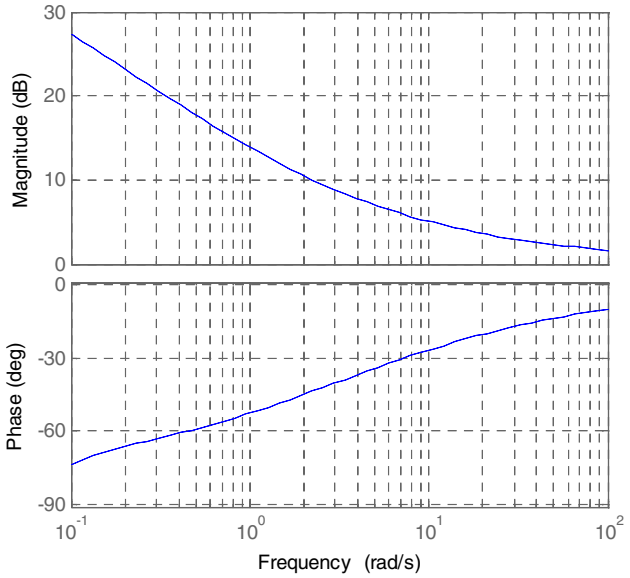

Fig. 9 Frequency-domain response for first individual channel

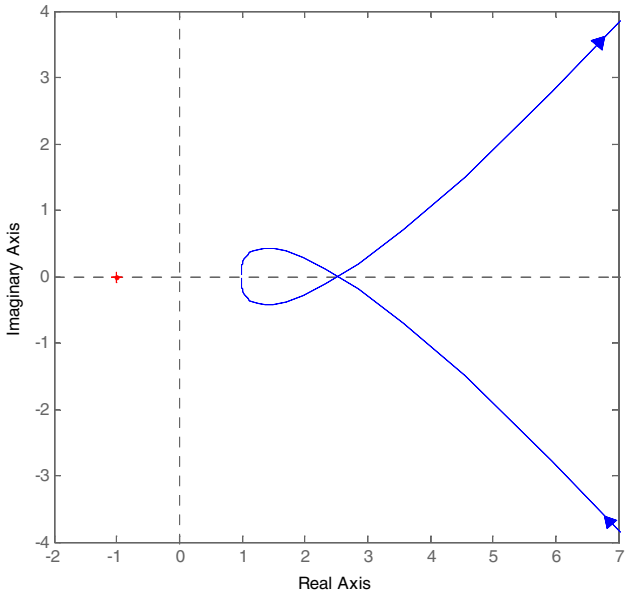

Fig. 11 Nyquist graph for the second individual channel

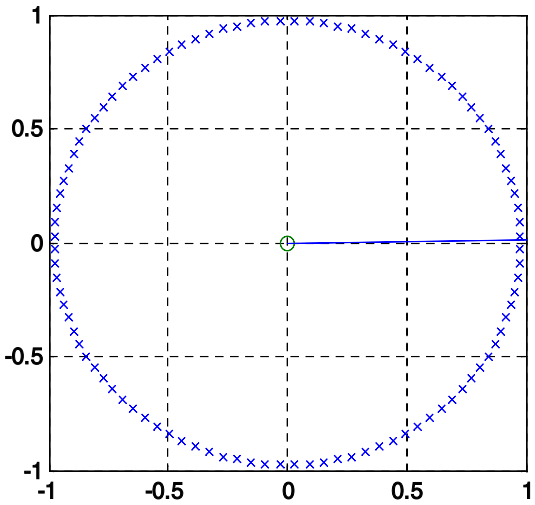

Fig. 10 Pole positions for the second individual channel

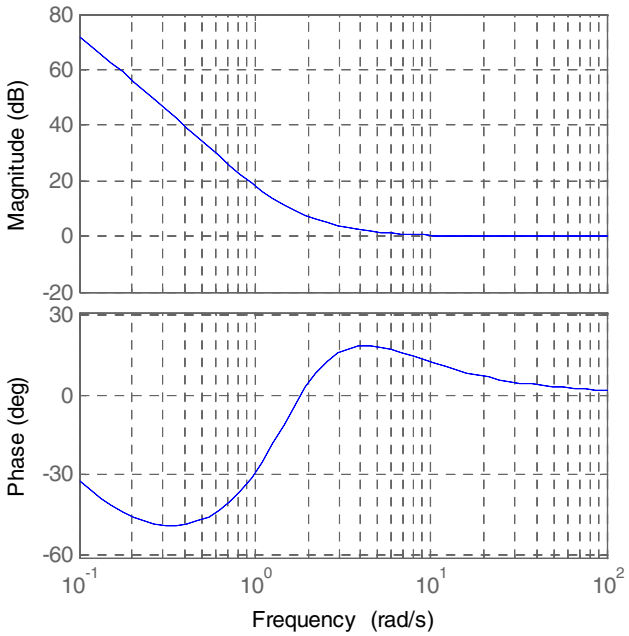

Fig. 12 Frequency-domain response for second individual channel

7.1 Platform Testing

After the autonomous ground vehicle's model and the two FOPID controllers have been implemented, the platform is simulated and examined through different case studies to verify the response of the proposed methodology. Each case considers a different path as follows:

Case Study-1

In this case, a circular smooth trajectory was generated as desired trajectory. Equation (44) was used to generate the orientation of the trajectory. This trajectory was compared with the actual trajectory to find the error. Hence, the error was fed into the fractional-order controller. The output of the fractional-order controller is presented the control action that was connected the motor of the left wheel. The second input represents the desired velocity. The latter equals to $v_d = 0.4[\text{m/sec}]$ for interval $0 \leq t \leq 40\,[rad]$. This velocity was compared with the actual velocity of the vehicle. The error produced by comparing the velocity was inputted to the second fractional-order controller. The output of the velocity controller was connected the motor of the left wheel. After running the simulation, the relationship between the desired and actual trajectory is shown in Fig. 13. Figure 14 depicts

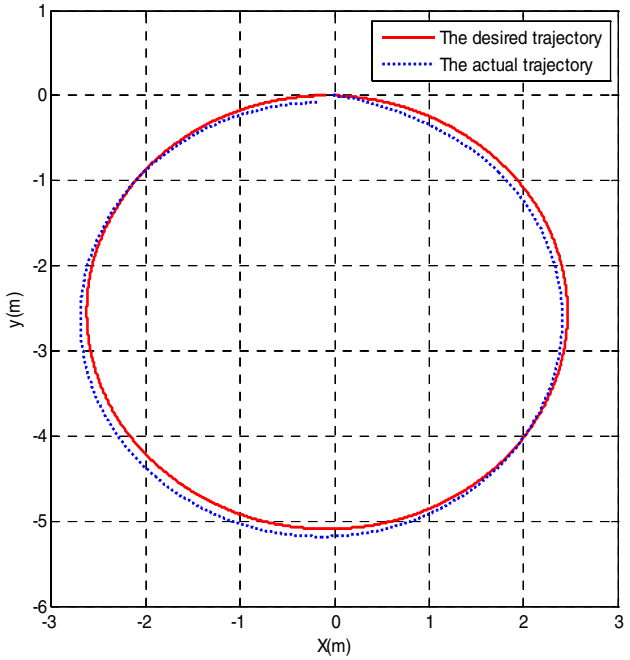

Fig. 13 The relationship between the desired and actual trajectories for the circular trajectory

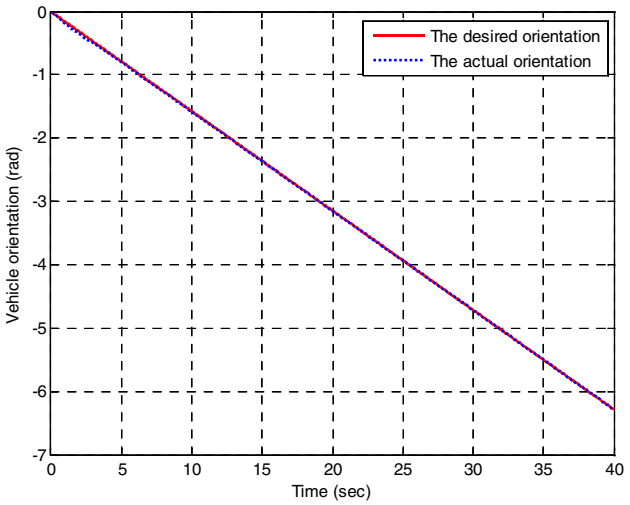

Fig. 14 The desired and actual orientation for the circular trajectory

the orientation of vehicle that was used for generating the circular trajectory. The error between the desired and the actual orientation is depicted in Fig. 15. Figure 16 shows the changing of the integral square error functions of both the orientation and velocity of the vehicle.

$$\theta_d = (2\pi t/-40)\,[rad]\,0 \leq t \leq 40\,[rad] \tag{44}$$

Case Study-2

In response to another case and to show the adaptation of the proposed controller, a linear trajectory was created. To ensure a linear trajectory, a constant orientation should

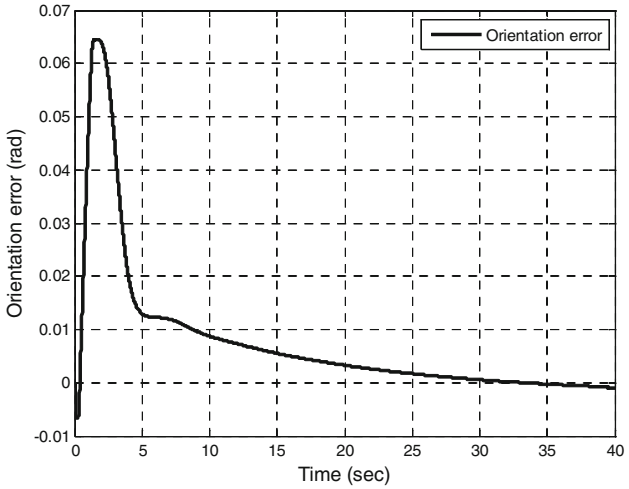

Fig. 15 The tracking error between the desired and actual orientation for the circular trajectory

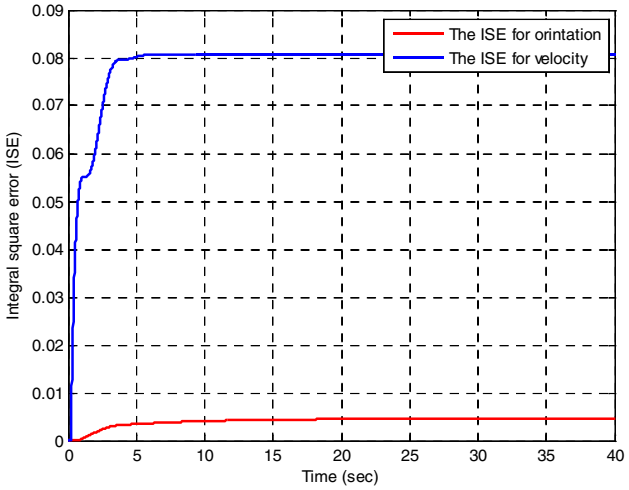

Fig. 16 The integral square error for the orientation and velocity of the vehicle for circular trajectory

be generated using $\theta_d = \pi/4\ [rad]$ for interval$0 \leq t \leq 40\,[sec]$. Similarly, the relationship between the desired and actual trajectory is shown in Fig. 17. Figure 18 depicts the vehicle orientation that was used for generating the linear trajectory. The error between the desired and the actual orientation is depicted in Fig. 19. Figure 20 shows the changing of the integral square error functions of both the orientation and velocity of the vehicle of linear trajectory.

The simulation results for the desired, actual and the error between them are shown in Fig. 21. The results are the same for both case studies because the desired velocity remained without changing in its value.

7.2 Robustness Analysis

Designing an accurate and robust control system in the presence of disturbances in the dynamic systems is a challenging

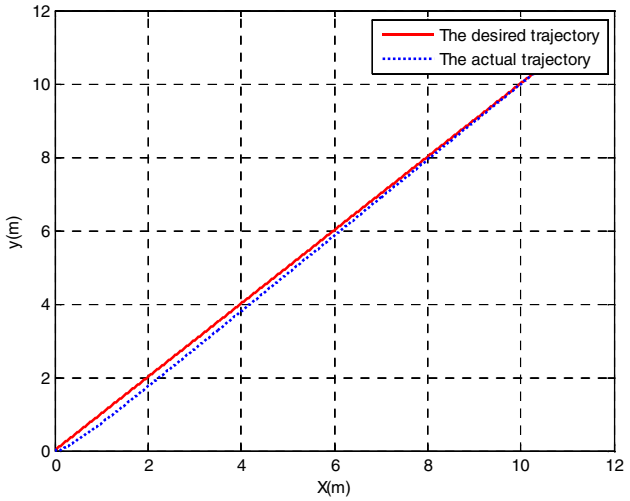

Fig. 17 The relationship between the desired and actual trajectories

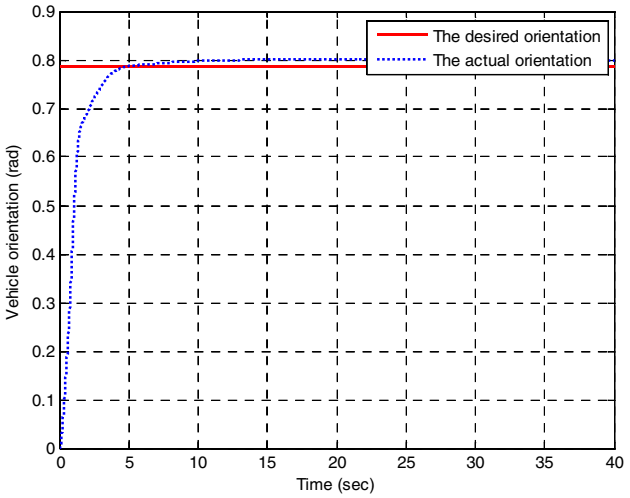

Fig. 18 The desired and actual orientation for the linear trajectory

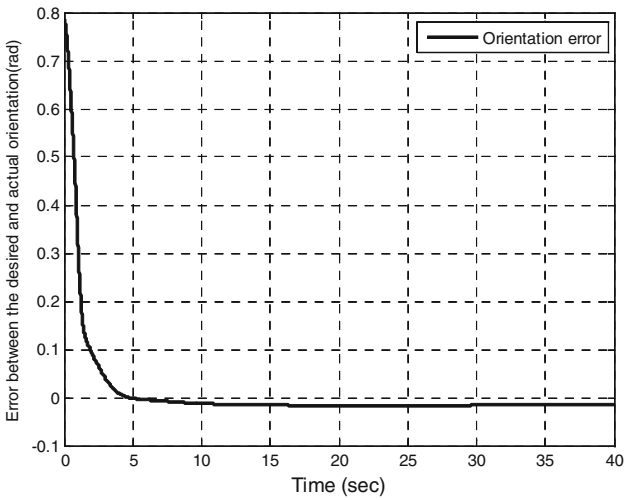

Fig. 19 The tracking error between the desired and actual orientation for the linear trajectory

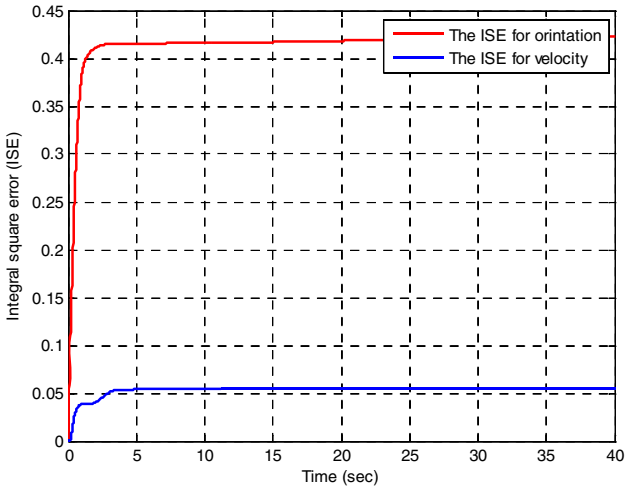

Fig. 20 The integral square error for the orientation and velocity of the vehicle for linear trajectory

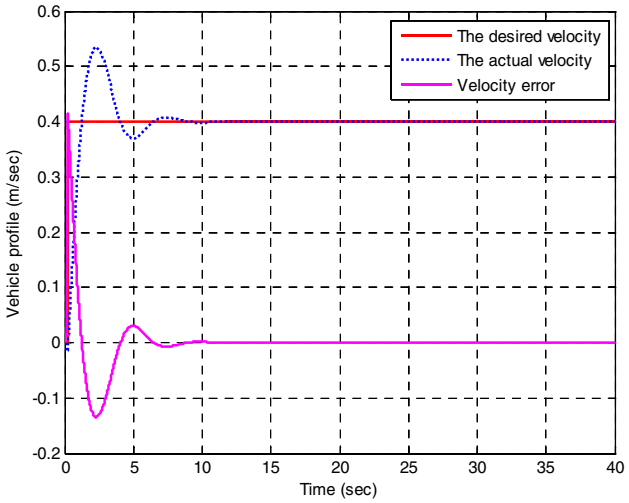

Fig. 21 The profile for desired, actual and error velocity for the circular linear trajectory

problem. Therefore, it is essential to test the parameters of fractional order to meet the performance specifications and have desirable robustness. In this paper, the robustness of the fractional-order PID controller is examined by applying disturbances due to the external friction produced form the vehicle motion between the wheels and ground. Figures 22 and 23 describe the time response of the mean square error of fractional-order PID controller for the orientation and velocity controller, respectively. In Fig. 22, the external disturbance is applied solely on the right wheel due to friction between the wheel and the ground and similarly in Fig. 23 due to the left wheel. It is apparent that there is a very slight change in the response if the disturbance is applied. However, the change will be observed if a large disturbance is enforced. The relationship between disturbances due to right

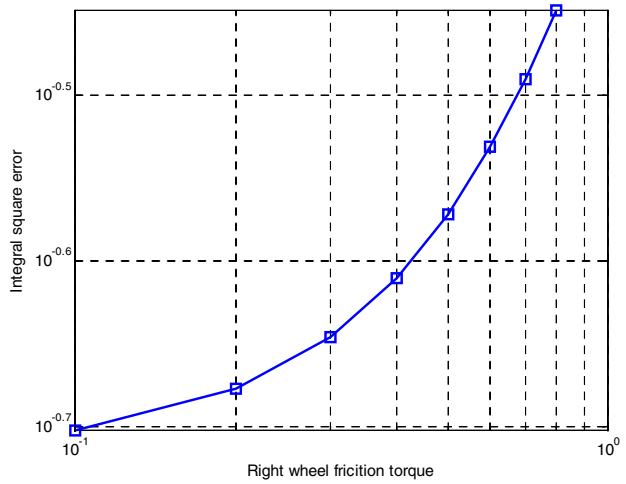

Fig. 22 Time response of ISE for the orientation controller against different amplitudes of right wheel friction torque

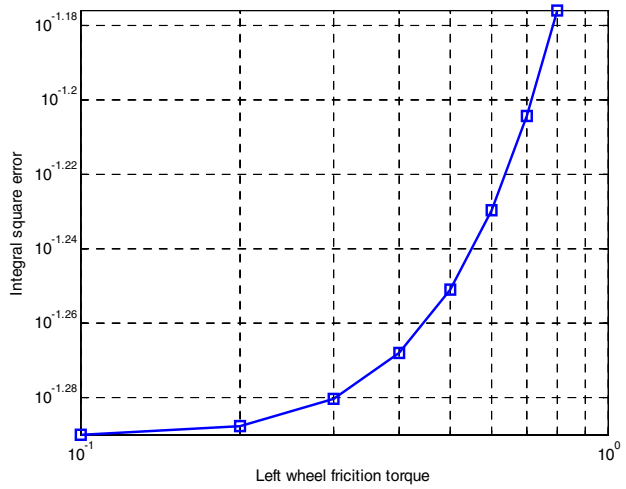

Fig. 23 Time response of ISE for the velocity controller against different amplitudes of left wheel friction torque

and left wheels friction against the integral square error is given in Table 6.

7.3 Comparison with Conventional PID Controller

In this section, a comparison between fractional-order PID and the conventional one is presented. The parameters of conventional PID controller for both orientation and velocity controller are given in Tables 7 and 8, respectively. These parameters were tuned in the same manner as in fractional-order PID aforementioned using particle swarm optimization technique. A comparison for the orientation tracking error for circular and linear trajectories is depicted in Figs. 24 and 25, respectively. It is clearly obvious that the fractional-order PID controller shows a significant improvement in terms of minimizing the tracking error.

Table 6 Disturbances due to wheels friction against integral square error

Friction due to right wheel	Friction due to left wheel	ISE for FOPID # 1	ISE for FOPID # 2
0	0	0.1924	0.05157
0.1	0	0.1986	0.05156
0.2	0	0.2103	0.05156
0.3	0	0.2260	0.05155
0.4	0	0.2452	0.05154
0.5	0	0.2679	0.05153
0.6	0	0.2939	0.05152
0.7	0	0.3232	0.05152
0.8	0	0.3557	0.05152
0.25	0.25	0.2180	0.05192
0.5	0.5	0.2695	0.05604
0.8	0.8	0.3606	0.06653

Table 7 Parameters of the conventional PID controller for AGV's orientation

Parameters	K_{p1}	K_{i1}	K_{d1}
Value	1.754	1.830	12.904

Table 8 Parameters of the conventional PID controller for AGV's velocity

Parameters	K_{p2}	K_{i2}	K_{d2}
Value	5.378	7.027	0.293

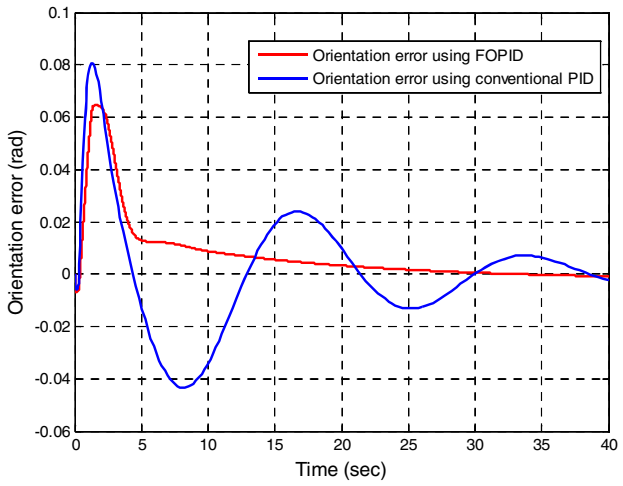

Fig. 24 The tracking error between the desired and actual orientation for the circular trajectory

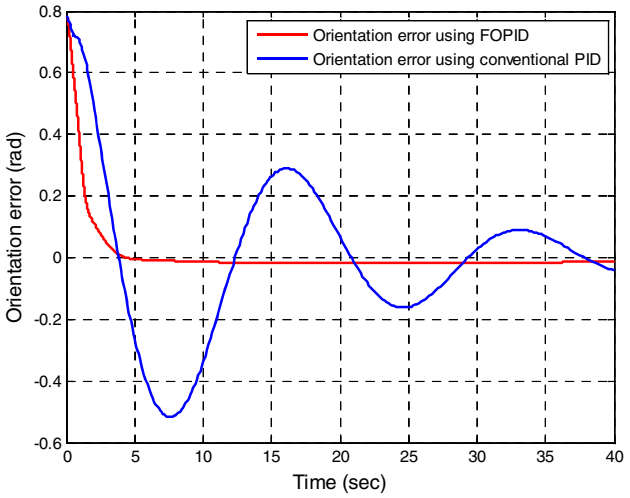

Fig. 25 The tracking error between the desired and actual orientation for the linear trajectory

8 Conclusion

Fractional-order $PI^{\lambda}D^{\mu}$ controller has been introduced to control the motion of the autonomous ground vehicle. This controller is optimized by minimizing the cost function. The particle swarm optimization algorithm has been used to tune the parameters of the FOPID controller. The designed FOPID controller has shown the significant ability of the autonomous ground vehicle to track the desired trajectory. Two different trajectories, i.e. circular and linear trajectories, are considered to test the adaptation of the system. The simulation results have confirmed successfully the effectiveness and validation of the proposed FOPID controller in terms of stability, trajectory tracking control, tracking error minimizing and robustness.

The effect of external disturbances has been taken into consideration to test the efficient and robustness of the proposed FOPID controller. The left and right wheel friction torques are changed when an external disturbance occurs. This change does not affect the vehicle operation even it is applied permanently. The results have shown without doubt the effectiveness and robustness of the proposed FOPID controller.

Acknowledgments The author would like to express his gratefulness for his sponsor, Ministry of Higher Education and Scientific Research in Iraq, for funding his research programme in the United Kingdom. The author would also like to thank his home university for the support, University of Basrah in Iraq.

References

Aboelela, Ma S, Ahmed, M. F., & Dorrah, H. T. (2012). Design of aerospace control systems using fractional PID controller. *Journal of Advanced Research*, *3*(3), 225–232.

Aldair, A. A., & Wang, W. J. (2010). Design of fractional order controller based on evolutionary algorithm for a full vehicle nonlinear active suspension systems. *International Journal of Control and Automation*, *3*(4), 33–46.

Al-Mayyahi, A., Wang, W., & Birch, P. (2015). Path tracking of autonomous ground vehicle based on fractional order PID controller optimized by PSO In *13th IEEE International Symposium on Applied Machine Intelligence and Informatics (SAMI)*, pp. 109–114.

Al-Mayyahi, A., Wang, W., & Birch, P. (2014). Adaptive neuro-fuzzy technique for autonomous ground vehicle navigation. *Robotics*, *3*(4), 349–370.

Cao, J., & Cao, B. (2006). Design of Fractional Order Controllers Based on Particle Swarm Optimization. In *1st IEEE Conference on Industrial Electronics and Applications*, pp. 1 – 6.

Cao, J., Liang, J. I. N., & Cao, B. (2005). Optimization of Fractional Order PID Controllers Based on Genetic Algorithms. In *The fourth International Conference on Machine Learning and Cybernetics*, pp. 5686–5689.

Chen, Y., Petr, I., & Xue, D. (2009). Fractional Order Control - A Tutorial, In *American Control Conference*, pp. 1397–1411.

Fierro, R., & Lewis, F. L. (1997). Control of a nonholonomic mobile robot?: Backstepping kinematics into dynamics. *Journal of Robotic Systems*, *14*(3), 149–163.

Fierro, R., & Lewis, F. L. (1998). Control of a nonholonomic mobile robot using neural networks. *IEEE Transactions on Neural Networks*, *9*(4), 589–600.

Huang, J., Wen, C., Wang, W., & Jiang, Z.-P. (2014). Adaptive output feedback tracking control of a nonholonomic mobile robot. *Automatica*, *50*(3), 821–831.

Lee, C.-H., & Chang, F.-K. (2010). Fractional-order PID controller optimization via improved electromagnetism-like algorithm. *Expert Systems with Applications*, *37*(12), 8871–8878.

Monje, C. A., Chen, Y., Vinagre, B. M., Xue, D., & Feliu, V. (2010). *Fractional-order systems and controls fundamentals and applications*. New York: Springer.

Normey-Rico, J. E., Alcalá, I., Gómez-Ortega, J., & Camacho, E. F. (2001). Mobile robot path tracking using a robust PID controller. *Control Engineering Practice*, *9*(11), 1209–1214.

Peng, J., Yu, J., & Wang, J. (2014). Robust adaptive tracking control for nonholonomic mobile manipulator with uncertainties. *ISA Transactions*, *53*(4), 1035–1043.

Ramezanian, H., & Balochian, S. (2013). Optimal design a fractional-order PID controller using particle swarm optimization algorithm. *International Journal of Control and Automation*, *6*(4), 55–68.

Resende, C. Z., Carelli, R., & Sarcinelli-Filho, M. (2013). A nonlinear trajectory tracking controller for mobile robots with velocity limitation via fuzzy gains. *Control Engineering Practice*, *21*(10), 1302–1309.

Ugalde-loo, C. E., Liceaga-castro, E., & Liceaga-castro, J. (2005). "2x2 Individual Channel Design MATLAB Toolbox, In *44th IEEE Conference on Decision and Control*, pp. 7603–7608.

Vivero, O., & Liceaga-Castro, J. (2008). MIMO Toolbox for Matlab, in Student Paper. *Annual IEEE Conference*, *2008*, pp. 1–5.

Wang, J., Lu, Z., Chen, W., & Wu, X. (2011). An Adaptive Trajectory Tracking Control of Wheeled Mobile Robots. In *The sixth IEEE Conference on Industrial Electronics and Applications*, 3, pp. 1156–1160.

Zamani, M., Karimi-Ghartemani, M., Sadati, N., & Parniani, M. (2009). Design of a fractional order PID controller for an AVR using particle swarm optimization. *Control Engineering Practice*, *17*(12), 1380–1387.

Zhang, Y., Gong, D., & Zhang, J. (2013). Robot path planning in uncertain environment using multi-objective particle swarm optimization. *Neurocomputing*, *103*, 172–185.

Zhang, Y., Liu, G., & Luo, B. (2014). Finite time cascaded tracking control approach for mobile robots. *Information Sciences*, *284*, 31–43.

Zhao, P., Chen, J., Song, Y., Tao, X., Xu, T., & Mei, T. (2012). Design of a control system for an autonomous vehicle based on adaptive-PID. *International Journal of Advanced Robotic Systems*, *9*(44), 1.